NASA Technical Memorandum 107152

Application of the Self Calibrating Emissivity and/or Transmissivity Independent Multiwavelength Pyrometer to Measure the Temperatures of Tungsten and Refractory Material Surfaces

Daniel Ng and Charles M. Spuckler
Lewis Research Center
Cleveland, Ohio

January 1996

National Aeronautics and
Space Administration

APPLICATION OF THE SELF CALIBRATING EMISSIVITY AND/OR TRANSMISSIVITY INDEPENDENT MULTIWAVELENGTH PYROMETER TO MEASURE THE TEMPERATURES OF TUNGSTEN AND REFRACTORY MATERIAL SURFACES

DANIEL NG
NASA Lewis Research Center
Cleveland, OH 44135

CHARLES M. SPUCKLER
NASA Lewis Research Center
Cleveland, OH 44135

Introduction

The self calibrating emissivity and/or transmissivity independent multiwavelength pyrometer is ideally suited to measure the temperature of a surface when the emissivity of the surface and the transmissivity of the medium separating the surface from the pyrometer are either or both not known. Such is the case of the tungsten filament in a quartz lamp. Using a one-color pyrometer would require knowing the quartz lamp envelope transmissivity and the filament's emissivity to measure temperature. This information can only be obtained if samples of the filament and envelope are available. Assuming that these quantities are wavelength independent over a wavelength region, a ratioing 2-color pyrometer can measure the temperature, but the ratio signal is susceptible to noise. The disappearing filament pyrometer measures only a brightness temperature. It still needs the emissivity and transmissivity to make corrections to the measured temperature. The NASA self calibrating multiwavelength pyrometer[1] is a recent addition to the list of pyrometers used in research and development. Its principle of operation makes it ideally suited to measure the temperature of surfaces without needing to know the emissivity of the surface, the transmissivity of the intervening medium or the calibration constant of the detector before hand. It has successfully measured the surface temperatures of tungsten, silicon carbide and refractory oxides in three infrared light sources. The measured temperatures are used to analyze the heat transfer in each case.

Method

Following the description in reference 1, voltage spectra of the three infrared light sources are measured using a multiwavelength pyrometer. Constant currents are sent through them to attain different temperatures. Emission of electromagnetic radiation takes place according to Planck's law. The voltage spectra $V(\lambda,T(t))$ of wavelengths $\lambda_1, \lambda_2, ..\lambda_s.. \lambda_N$, at times $t_1, t_2, .. t_i, .. t_n$, are recorded. At those times, the temperatures $T(t_1)\neq T(t_2)\neq .. \neq T(t_i)\neq ..\neq T(t_n)$, are not known. The filament spectral emissivity, ε_λ, the glass envelope spectral transmissivity, τ_λ, and the pyrometer calibration constant, g_λ, are all unknown, but are assumed to be constant. The basics of the self calibrating pyrometer are contained in three equations[1] (Eqns. 1-3) connects two wavelengths, labeled λ_R and λ_I.

$$V(\lambda_I, t) = g_I \varepsilon_I \tau_I \left\{ \frac{\frac{C_1}{\lambda_I^5}}{\left(\frac{C_1/\lambda_R^5}{V(\lambda_R, t)/g_R \varepsilon_R \tau_R} + 1 \right)^{\frac{\lambda_R}{\lambda_I}} - 1} \right\} \tag{1}$$

$$T(\lambda, t) = \frac{C_2/\lambda_I}{Log_e\left(g_I \varepsilon_I \tau_I \frac{C_1}{\lambda_I^5} \frac{1}{V(\lambda_I, t)} + 1 \right)} \tag{2}$$

$$T(t)=\frac{\sum_{I=1}^{I=N} T(\lambda_I, t)}{N} \tag{3}$$

With the determination of a single number, $g_R\varepsilon_R\tau_R$, all the other $g_I\varepsilon_I\tau_I$ and temperatures T(t) are automatically determined in terms of it. The value of $g_R\varepsilon_R\tau_R$ is determined using a variational least squares method. Begin by assuming a value for $g_R\varepsilon_R\tau_R$, plotting the quantity on the left hand side of Eqn. 1 vs the quantity inside the curly bracket on the right hand side gives a straight line with slope of $g_I\varepsilon_I\tau_I$. Do this for all I≠R to determine $g_I\varepsilon_I\tau_I$ which are used to calculate the average temperatures T(t).

In the application of multiwavelength pyrometry to measure the temperatures of these surfaces, difference spectra D(λ,T(t)) are obtained when a voltage spectrum at temperature T_r=T(t_r)) is taken as reference and subtracted from all the spectra, including itself.

$$D(\lambda, T(t)) = V(\lambda, T(t)) - V(\lambda, T(t_r)) \tag{4}$$

Spectra produced by the multiwavelength pyrometer are themselves voltage differences when the detector is alternated to look at the measured surface and at an internal black body reference. The transformation (Eqn. 4) introduces another unknown T_r to be determined. Making use of the fact that

$$V(\lambda, T(t)) = g_\lambda \varepsilon_\lambda \tau_\lambda L(\lambda, T(t)) = g_\lambda \varepsilon_\lambda \tau_\lambda \frac{c_1}{\lambda^5} \frac{1}{\exp(c_2/\lambda T(t)) - 1} \tag{5}$$

Eqns. 1 and 2 now become

$$D(\lambda_I, t) = g_I \varepsilon_I \tau_I \left\{ \frac{\frac{c_1}{\lambda_I^5}}{\left(\frac{c_1/\lambda_R^5}{L(\lambda_R, T_r) + D(\lambda_R, t)/g_R\varepsilon_R\tau_R} + 1 \right)^{\frac{\lambda_R}{\lambda_I}} - 1} \right\} - g_I \varepsilon_I \tau_I L(\lambda_I, T_r) \tag{6}$$

$$T(\lambda, t) = \frac{c_2/\lambda_I}{Log_e\left(\frac{c_1}{\lambda_I^5} \frac{1}{L(\lambda_I, T_r) + D(\lambda_I, t)/g_I\varepsilon_I\tau_I} + 1 \right)} \tag{7}$$

Referring to Eqn. 6, assigning a value to $g_R\varepsilon_R\tau_R$ and to T_r in Eqn. 6, the quantity inside the curly bracket on the right hand side is evaluated and plotted against the quantity on the left hand side. A straight line is obtained. A standard least squares method is used to determine its slope, which is $g_I\varepsilon_I\tau_I$. A variational least squares procedure is used to determine $g_R\varepsilon_R\tau_R$ and T_r as follows:

1) Choose a value for T_r.
2) Choose a wavelength for λ_R and a wavelength for λ_I and a value for $g_R\varepsilon_R\tau_R$.
3) Plot the data according to Eqn. 6 to determine the $g_I\varepsilon_I\tau_I$ from the slopes.
4) Do so for all I≠R.
5) Use the determined $g_I\varepsilon_I\tau_I$ to calculate the temperatures T(t) according to Eqns. 6, 7 and 3.
6) Transform the spectra $V(\lambda_I,t)$ into a single large data set (x,y). The wavelength λ_I is transformed into $c_2/\lambda_I T(t)$, the voltage $V(\lambda_I,t)$ is transformed by first dividing by $g_I\varepsilon_I\tau_I$ and then by $T(t)^5$, the 5th power of the spectrum temperature, according to

$$x = \frac{c_2}{\lambda T(t)} \quad , \quad y = \frac{L(\lambda, T_r) + D(\lambda, t)/g\varepsilon\tau}{T(t)^5} = \frac{c_1}{c_2^5} \frac{x^5}{e^x - 1} \tag{8}$$

7) The transformed (x,y) data obey the generalized non-dimensional Planck function (Eqn. 8), an invariant curve. The (x,y) data are fitted to this function by calculating the residual Σ, defined

as the sum of the squares of the difference between the transformed y_I and the calculated y evaluated by substituting the transformed x_I in the y equation in Eqn. 8 for all the data.

8) A new value for $g_R\varepsilon_R\tau_R$ is selected, and steps (2 to 7) repeated.
9) The value of $g_R\varepsilon_R\tau_R$ that produced the least Σ is recorded.
10) Choose a new value for T_r, repeat steps (2 to 9).
11) The combination of $g_R\varepsilon_R\tau_R$ and T_r that produced the least over all Σ is the correct one we seek.

With $g_R\varepsilon_R\tau_R$ and T_r determined, all the T(t) are also determined. In one stroke, everything that is needed in pyrometry for temperature measurement is determined. Temperatures at any time in the past or in the future are determined from each λ according to Eqn 3 or by least squares curve fitting. As is evident, the pyrometer requires no prior calibration. The procedures (1 to 11) can be repeated as often as necessary during an experiment to update the self calibrating process.

1 Tungsten filament Results

The quartz lamp used is a commercial Oriel 6333 QTH lamp. Voltage spectra obtained from it are shown in figure 1 for the 0.5 and 2.5 μm spectral region. Above 2.5 μm the intensity is very low. These spectra correspond to different input power (15 to 90 watts) delivered by a stable power supply to the quartz lamp. The multiwavelength pyrometer uses two detectors to obtain these spectra. They are silicon (0.4 μm $<\lambda<$ 1.2 μm) and lead sulphide ($\lambda >$1.2 μm) detectors. The detectivity of the lead sulphide detector is much less than that of silicon. The spectra detected by lead sulphide in this region is shown at a different scale in figure 2. The spectrometer is positioned 3 meters away from the lamp, operating at 0.5 mR (milliradian) field of view. The minima in figure 1 are due to absorption by the atmosphere and the quartz envelope in the optical path between the detector and the filament. Following the analysis above, difference spectra are formed (figure 3). λ_R is chosen to be 1 μm. Figure 4 shows the case of λ_R=1 μm, λ_I=0.8 μm, $g_R\varepsilon_R\tau_R$=0.0142, and T_r=3280.1 K. It is indeed a straight line. The slope (i.e. $g_I\varepsilon_I\tau_I$) of plots like this at other wavelengths are obtained using a least squares method and are plotted in figure 5. These $g_I\varepsilon_I\tau_I$ are now used to calculate the temperature of each spectrum according to Eqn. 7 and by the variation procedure described above to determine $g_R\varepsilon_R\tau_R$ and the temperatures. The final calculated temperatures are shown in figure 6. They are almost independent of wavelength. Their averages at 15, 30, 45, 60, 75 and 90 watts input are 1960, 2398, 2704, 2934, 3112 and 3280 K. The nominal temperature of the quartz lamp at 100 watts is 3400 K. The least squares fitting of the data to the generalized Planck function are shown in figure 7. The filament temperatures were also measured by an inexperienced user of a disappearing filament pyrometer looking through the lamp's quartz envelope. The temperatures obtained (1738, 1973, 2383, 2553, 2743 and 2983 K) are shown together with the pyrometer measured values in figure 8 as a function of the input power. As expected, the two measurements are not equal because the lamp envelope's transmissivity and the filament's emissivity are not factored in by the disappearing filament pyrometer, which effectively considered both to be equal to unity. But the trend of temperature changes with input power is noticeably similar.

We correct the disappearing filament pyrometer temperature using the simplified analysis that follows. Treating the filament as a small object of uniform temperature with two lead wires, the input power is dissipated by convection and radiation from its surfaces and conduction down the lead wires

$$P=A_1 h\,(T-T_0)+2A_2\kappa\left(\frac{T-T_0}{L}\right)+A_3\tau\varepsilon\sigma\,(T^4-T_0^4) \qquad (9)$$

where A_1 is the convective surface area of the filament, A_2 is the conductive cross-sectional area of the lead wires, A_3 is the radiating surface area, h is the heat transfer coefficient, κ is the thermal conductivity, τ is the transmission coefficient of the lamp envelope, ε the emissivity of the filament surface, L=10 mm is the length of the lead wires, σ is the Stefan-Boltzmann radiation constant, and T_0 is the ambient temperature. The temperature of the gas inside the quartz lamp and the temperature of the cold end of the lead wires are assumed to be T_0 for simplicity in the analysis. The quartz lamp filament consists of 10 turns of closely spaced tungsten wire coiled in the form of a hollow rectangular tube, measuring approximately 1 x 1.8 x 3.5 mm. In operating the pyrometer at a

distance of 3 meter from the filament at a field of view of 0.5 mR, the visible portion of the filament is only 1.5 mm, slightly smaller than the filament dimension. The total length of wire is approximately 56 mm, and the diameter of the wire is approximately 0.35 mm with an approximate total external surface area A=60 mm^2. It is assumed that half of the wires circumferential area is radiating to the surroundings, so this area is approximately 30 mm^2. This is the radiating surface A_3=30 mm^2. Eqn. 9 is written as

$$\frac{P}{T-T_0}=hA_1+\frac{2\kappa A_2}{L}+\tau\varepsilon\left\{\sigma A_3\frac{(T^4-T_0^4)}{T-T_0}\right\} \qquad (10)$$

Plotting the quantity on the left hand side vs the quantity inside the curly bracket on the right hand side in Eqn. 10 produced a straight line (figure 9). The slope of the straight line in figure 9 equals 0.404. It is the product of emissivity and transmissivity. The disappearing filament pyrometer operates with a red filter, taken to be at λ=0.7 μm. Correction to the observed temperature is given by

$$\frac{1}{T_c}=\frac{1}{T_{obs}}+\frac{\lambda}{c_2}\ln(\tau\varepsilon) \qquad (11)$$

Using the slope of the curve in figure 9 as the product $\tau\varepsilon$, the corrected temperature T_c is obtained from observed temperature T_{obs} according to Eqn. 11 and is plotted with the multiwavelength pyrometer measured temperature in figure 10. The agreement is satisfactory. The intercept of figure 9 is $hA_1+2A_2\kappa/L$=0.00297. Taking A_1=A=60 mm^2, and assuming the thermal conductivity of tungsten is 110 $Wm^{-1}K^{-1}$, this gives a heat transfer coefficient of 14.22 $Wm^{-2}K^{-1}$.

2 Silicon Carbide Heater Results

The silicon carbide heating element is sold by Oriel as catalog number 6573. It is a carborundum rod measuring 6 mm in diameter 10 cm long held in place by two brass receptacles at each end separated by 9 cm serving also as electrical contacts. Data were collected in exactly the same manner as for the quartz lamp. Different currents were sent through by the power supply which also indicated the total power being delivered across the heater. Because the metallic contacts at each end acted as a heat sinks and the large physical length over which the electrical energy is dissipated, larger temperature variations would exist near the ends of the heater. The hottest spot is at the center where the temperature is expected to be more uniform. The multiwavelength pyrometer was positioned so that it is accepting radiation from this hottest central region. The SiC heater spectra in the 1.3 and 14.5 μm spectral region are shown in figure 11 for different input current and power. The pyrometer used liquid nitrogen cooled indium antimonide (InSb) and mercury cadmium telluride (MCT) detectors. The MCT measured spectra are shown with a different scale in figure 12. The current and power used when these spectra were recorded are 3.2, 4.3, 5.4, 6.5, 7.6 and 8.4 A, and 30, 45, 60, 75, 90 and 115 watts respectively. These spectra are analyzed exactly as in the quartz filament case to obtain the temperatures (figure 13) and the calibration constants (figure 14). The spectrally averaged SiC surface temperatures at these input powers are 1070, 1012, 920, 819, 714 and 604 K. Also shown in figure 14 is the pyrometer's calibration constant measured from a separate experiment using a black body furnace. The ratio of the two curves gives the spectral emissivity of the SiC heater (figure 15).

The area sampled by the pyrometer is small compared to the dimension of the SiC rod. The center portion of the rod has the highest temperature. Assuming that the temperature in the measured region is uniform, conduction can be neglected. Numerical modeling of the longitudinal temperature variation at the center of the heater showed that it is very small. Therefore axial conduction is neglected. For this case the conduction term, $2A\kappa/L$ in Equation 10 is dropped. Consider a length dz of the heater that the pyrometer is observing. A current I is passed through it. This length has a resistance $dR=\rho dz/\pi r^2$. The power P generated by the passage of a current I is

$$P=I^2dR=\rho I^2\frac{dz}{\pi r^2} \qquad (12)$$

where ρ is the SiC electrical resistivity, and r is the radius of the SiC rod. A=2πrdz is the surface area over which the dissipated electrical energy is emitted and convected away. Eqn. 10 neglecting conduction becomes

$$\frac{I^2}{T-T_0}=\frac{2\pi^2 r^3}{\rho}h+\frac{\varepsilon\tau}{\rho}\left\{2\pi^2 r^3\sigma\frac{T^4-T_0^4}{T-T_0}\right\} \qquad (13)$$

Plotting the quantity on the left hand side of Eqn. 13 vs the quantity inside the curly bracket also gives a straight line (figure 16), with slope $\varepsilon\tau/\rho$ = 1467.3 and intercept $2\pi^2r^3h/\rho$=0.017. The resistivity ρ (neglecting temperature dependency) is obtained from figure 17 by plotting the input power (current times voltage) vs the square of the input current according to

$$P=RI^2=\rho\frac{L}{\pi r^2}I^2 \qquad (14)$$

where L is the length of the heater rod between electrical contacts and r its radius. The result is ρ = 0.000534 Ω-m, and $\varepsilon\tau$=0.78, which is consistent with the spectral emissivity shown in figure 15, if $\tau\approx1$. The heat transfer coefficient is found to be 17 $WK^{-1}m^{-2}$.

3 Ceramic Refractory Oxide Heater Results

The ceramic heater is an Oriel 6575. It is a heater constructed of a small ceramic (alumina) rod, wound with platinum resistance wire and then over coated with a mixture of the oxides of the rare earths. One end of the rod is exposed to air, the other is attached to a base plate. To measure temperature, the pyrometer is focused to a point roughly in the middle of the rod. Temperature was measured as before. The diameter of the heater is about 3 mm, its length is 14 mm. Electrical currents were passed through the wire to raise the temperature. Spectra were recorded (figure 18) and analyzed to obtain the temperatures (figure 19) and the calibration constants (figure 20) as before. The same black body calibration constants shown in figure 14 is also reproduced in figure 20. The average temperatures were determined to be 1646.5, 1381.3, 1147.27, 928.9, 720.4 and 539.5 K when the currents passed through were 7.0, 6.4, 5.8, 5.2, 4.6, 4 amps at 3.5, 3.0, 2.5, 2.2, 2.0 and 1.5 volts for a total power dissipation of 24.5, 19.2, 14.5, 11.44, 9.2 and 6 watts.

Following on the analysis of the SiC heater, the ceramic heater resistance is determined by plotting the input power vs the square of the input current (figure 21). Since the diameter of wire is not known, a resistance per unit length of heater is used. The total resistance is 0.463 ohm, giving a resistivity ρ=33.07 Ωm^{-1}. With some modification and neglecting conduction, the dissipated power and temperature will be plotted according to Eqn. 10. The power dissipated by the passage of a current through a length dz that has resistance dR=ρdz is given by

$$P=I^2dR=\rho I^2dz \qquad (15)$$

If the power is now dissipated over an area A=2πrdz. Eqn. 13, can be written as

$$\frac{I^2}{T-T_0}=\frac{2\pi r}{\rho}h+\frac{\varepsilon\tau}{\rho}\left\{2\pi r\sigma\frac{T^4-T_0^4}{T-T_0}\right\} \qquad (16)$$

Plotting the quantity on the left vs the quantity inside the curly bracket (fig 22) does not produce the expected linear relationship. Instead, plotting $I^2/(T-T_0)$ vs $1/(T-T_0)$ in figure 23, resulted in a curve that is more approximately a straight line.

The construction of the heater is such that the heat produced by the platinum wire is conducted out through the over coating and axially (or longitudinally) to the ends. The platinum resistance wire can be treated as an electrical heating shell of diameter r, and thickness d, where d is the diameter of the platinum wire. The heat energy $I^2dR=I^2\rho dz$ in length dz is conducted away at the rate of -k(dT/dr) radially from the heat generating resistance shell into the over coating material, and longitudinally at the rate of $-P_z$ per unit area from one end and P_{z+dz} per unit area from the other end of the element

length dz. The heat generated in this length, $I^2dR=I^2\kappa dz$ is dissipated by conduction along the rod and conduction radially out to the surface where it is convected and radiated away. This is written as

$$\rho I^2 dz = 2\pi r_0 h dz (T-T_0) + 2\pi r_0 dz \varepsilon\sigma (T_s^4 - T_0^4) + (P_{z+dz} - P_z)\pi r_0^2 \qquad (17)$$

where P_z and P_{z+dz} are longitudinal heat flux at the ends of the element dz, and r_0 is the radius at the heater surface. The heat conducted radially to the surface is

$$-\kappa\left(\frac{dT}{dr}\right)_{r_0} 2\pi r_0 dz = 2\pi r_0 dz\{h(T_s - T_0) + \varepsilon\sigma (T_s^4 - T_0^4)\} \qquad (18)$$

We obtained the ceramic emissivity (figure 24) from the ratio of the black body furnace calibration constant and the ceramic heater calibration constant both plotted in figure 20. Figure 24 shows well the behavior of non-gray emissivity ceramics. The emissivity is very low at short wavelengths and increases to higher values at the longer wavelengths. Thus, use of the Stefan-Boltzmann equation in Eqns. 17 and 18, assuming a constant emissivity at all wavelengths, is not a good estimate of the radiated power. The correct estimate is the integral P_r

$$P_r = \frac{c_1}{\lambda^5}\int_0^\infty \left(\frac{1}{\exp(c_2/\lambda T) - 1} - \frac{1}{\exp(c_2/\lambda T_0) - 1}\right) \varepsilon(\lambda)\tau(\lambda)\, d\lambda \qquad (19)$$

The radiation spectrum emitted by an ideal black body at temperature 1646 K and that emitted by the ceramic heater at the same temperature (obtained by multiplying the black body spectrum with the ceramic emissivity in figure 24) are shown in figure 25. At the same temperature, the ceramic heater radiates much less than a black body. The total energy emitted is given by the areas under the two curves. We numerically integrated them, using simple trapezoidal method between wavelengths. The integration from zero wavelength to the first wavelength channel is approximated by a triangle and integration after the last wavelength channel is truncated. The error in the integral of the black body curve compared with the Stefan-Boltzmann formula is about 10%. Integrating in this way, at the temperatures of the ceramic heater, the total net emitted power P_r are evaluated to be 3.259, 2.121, 1.337, 0.772, 0.374 and 0.141 watt/cm^2, being about 1/10 of that given by the Stefan-Boltzmann formula at the higher temperatures. This explains why the analysis of figure 22 failed. We now combine Eqns. 17, and 19, i.e. replacing $\varepsilon\sigma(T_s^4 - T_s^4)$ with Eqn. 19 to obtain

$$\rho I^2 dz = 2\pi r_0 h dz (T-T_0) + 2\pi r_0 dz P_r + \pi r_0^2 (P_{z+dz} - P_z) \qquad (20)$$

which can be rewritten as

$$\frac{\rho\frac{I^2}{2\pi r_0} - P_r}{T-T_0} = h + \frac{r_0}{2}\left(\frac{P_{z+dz} - P_z}{dz}\right)_{dz\to 0}\frac{1}{T-T_0} \qquad (21)$$

The temperature and input power data are now plotted according to Eqn. 21 (figure 26) resulting in a straight line. The intercept is 80 Wm^{-2}K^{-1} and the slope $(r_0/2)(\delta P_z/\delta z)$ = 35.92 kWm^{-2}.

Conclusion

The multiwavelength pyrometer successfully measured the temperatures of tungsten, silicon carbide and refractory oxides in infrared light sources without knowing the emissivity nor the transmissivity of intervening media. The measured temperatures were used to determine heat transfer parameters describing the experimental situations. The multiwavelength pyrometer itself was also not previously calibrated with any black body furnace of known temperature.

References

1 Ng, Daniel, Self Calibrating emissivity and/or transmissivity independent multiwavelength

pyrometer, NASA TM107149 E-Number 10087, 1996.

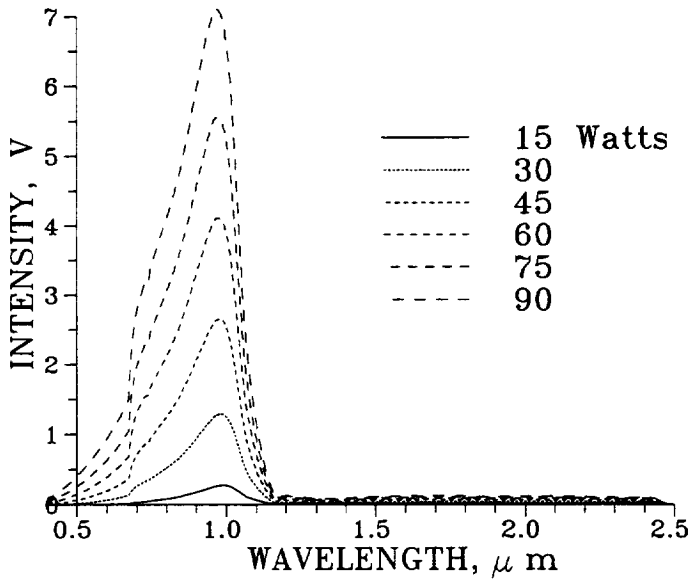

Figure 1
Spectra of Quartz lamp filament at different input powers.

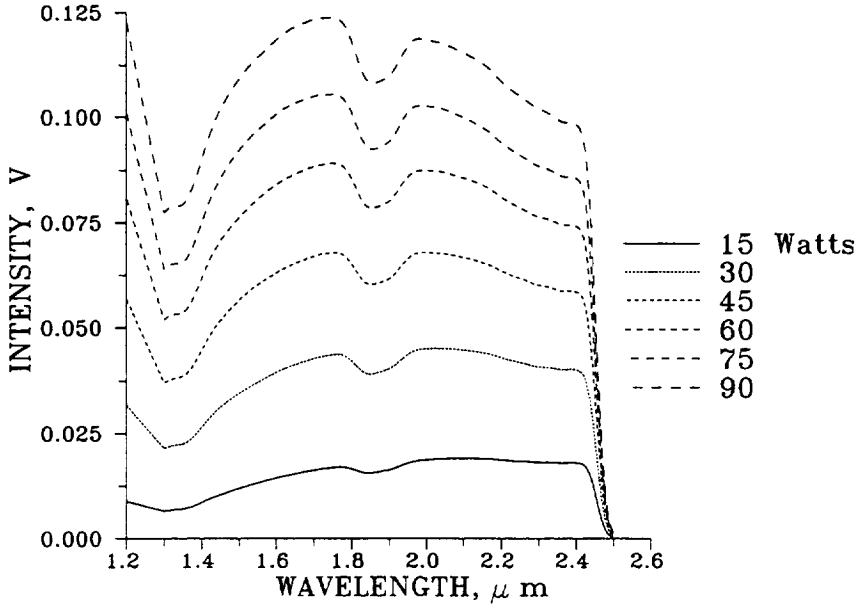

Figure 2
Expanded Scale of quartz lamp filament spectra in the 1.2 to 2.5 μm region.

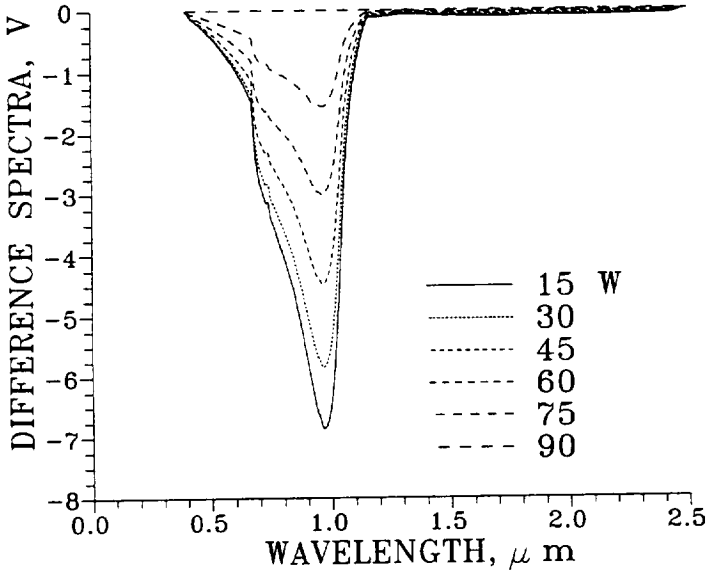

Figure 3
Difference spectra of tungsten filament at different input referenced to 90 W input.

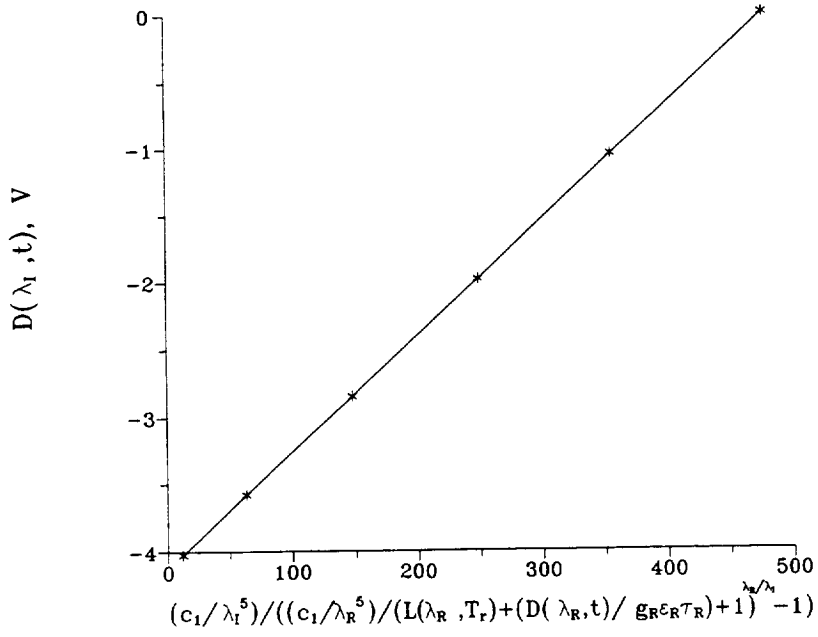

Figure 4
Plot of data to determine slope according to Eqn. 5, λ_I=0.8 μm, λ_R=1 μm, $g_R\varepsilon_R\tau_R$=0.0142, T_r=3280.1 K.

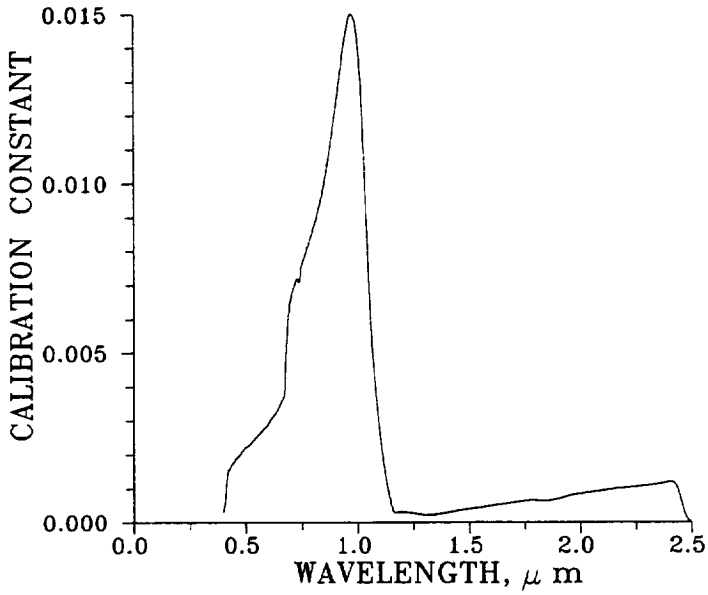

Figure 5
Calibration constants.

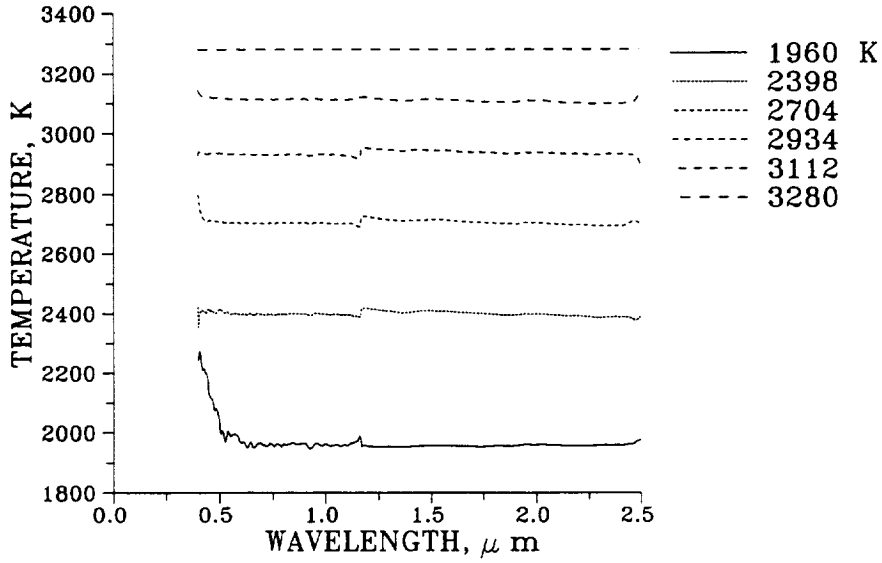

Figure 6
Calculated temperatures use the determined calibration constants.

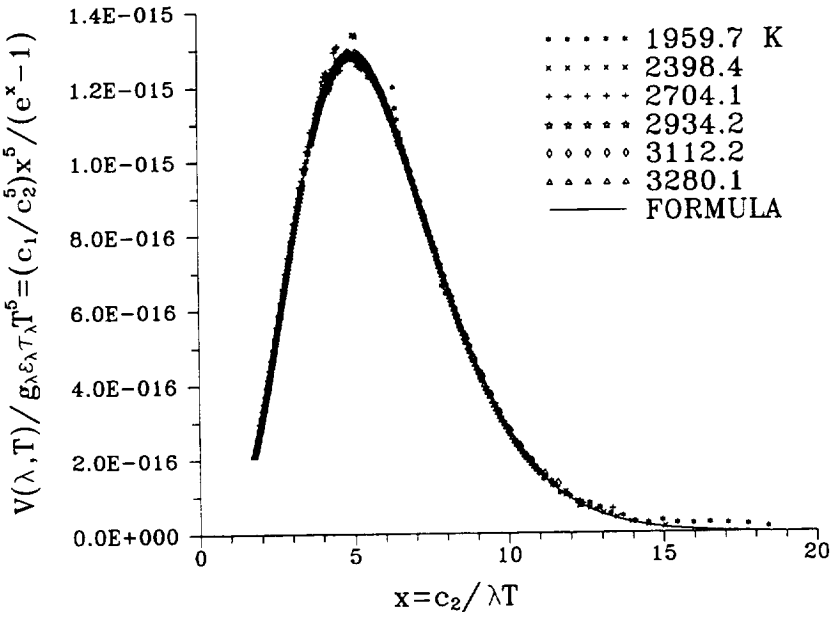

Figure 7
Least squares curve fitting of the transformed data to the non-dimensional Planck function.

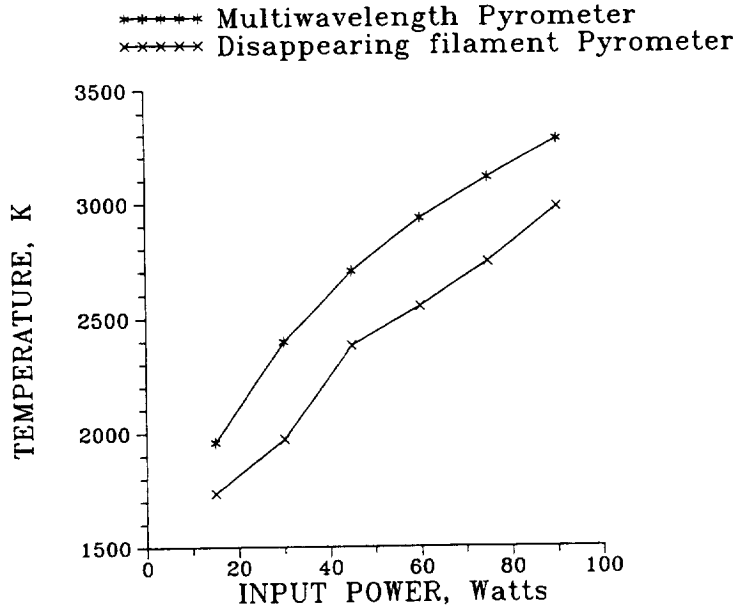

Figure 8
Plot of multiwavelength pyrometer and disappearing filament pyrometer temperatures at different input powers.

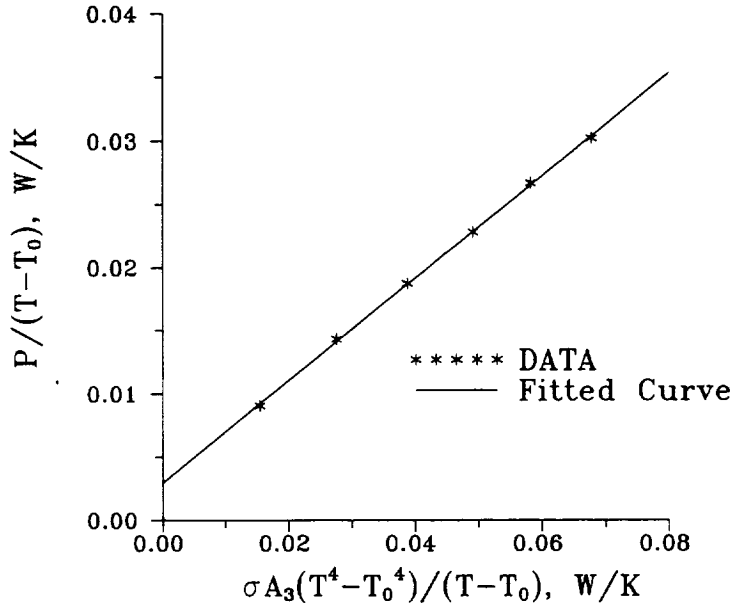

Figure 9
Plot of $P/(T-T_0)$ vs $\sigma A_3(T^4-T_0^4)/(T-T_0)$.

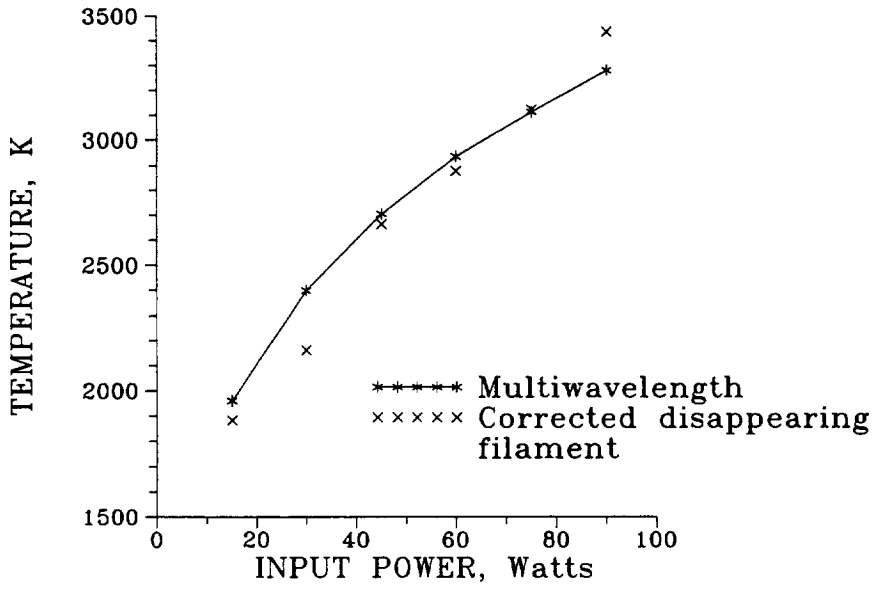

Figure 10
Plot of multiwavelength pyrometer and corrected disappearing filament pyrometer temperatures at different input powers.

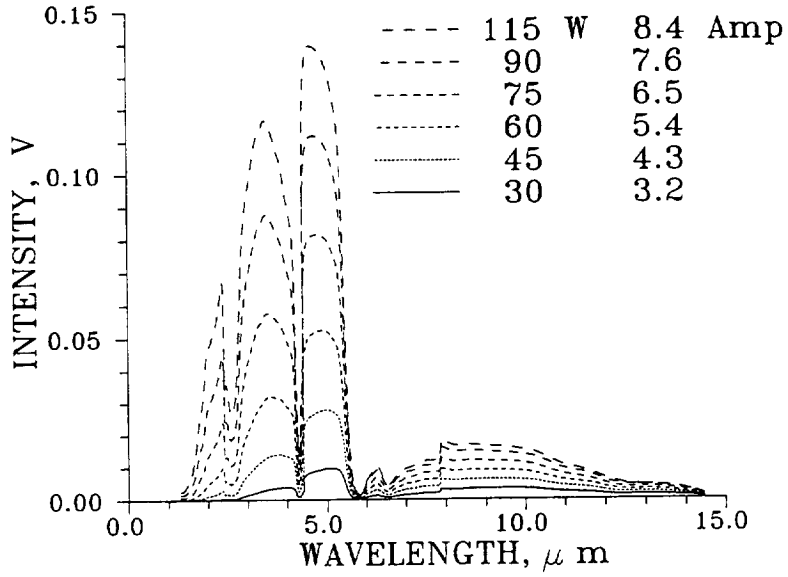

Figure 11
Spectra of SiC heater at different input powers.

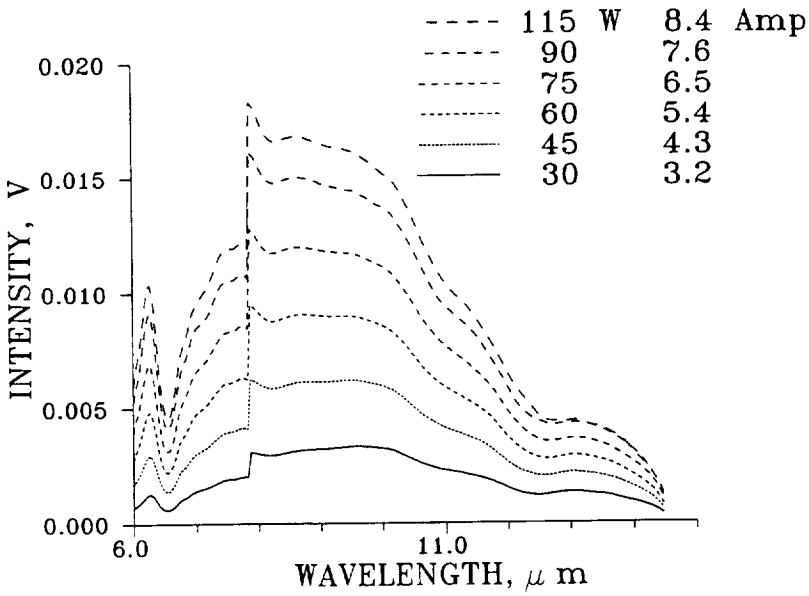

Figure 12
Expanded Scale of silicon carbide heater spectra in the 6 to 14.5 μm region.

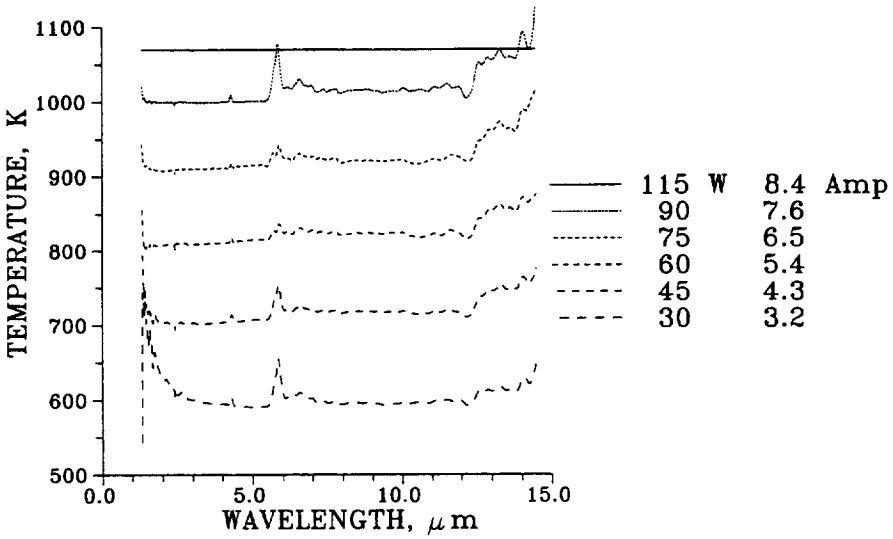

Figure 13
Calculated temperatures of the SiC heater use the determined calibration constants.

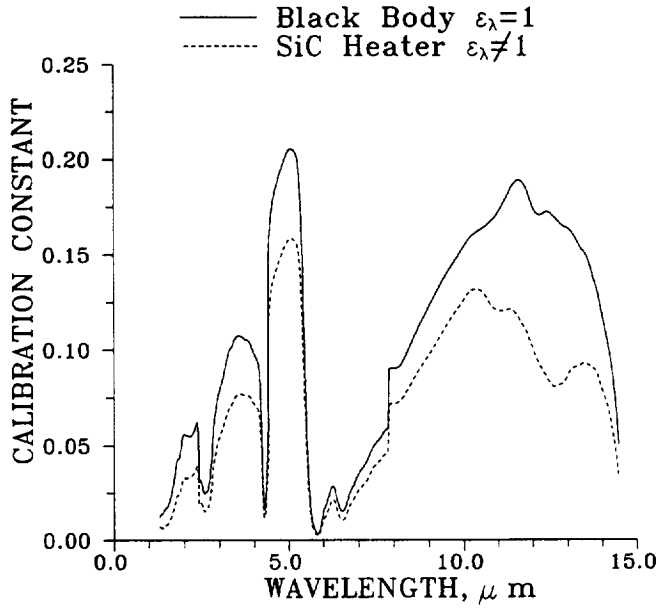

Figure 14
Multiwavelength pyrometer calibration constants with ε_λ=1 (black body) and $\varepsilon_\lambda \neq 1$ (SiC heater).

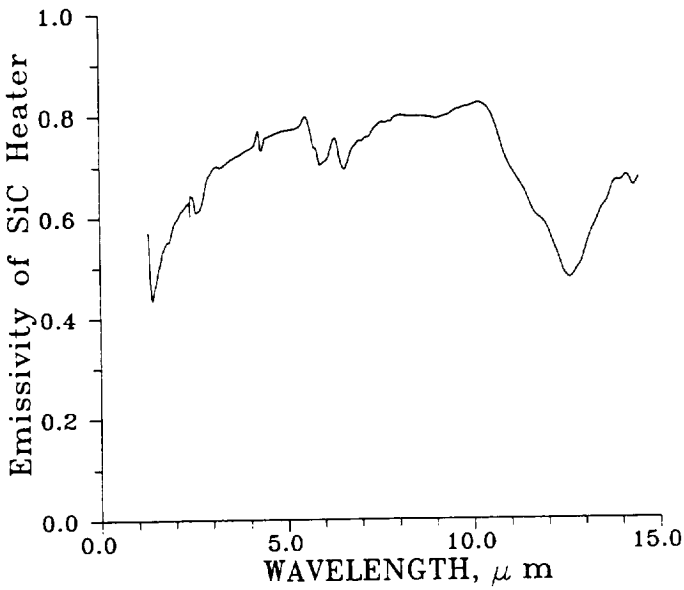

Figure 15
Emissivity of silicon carbide heater.

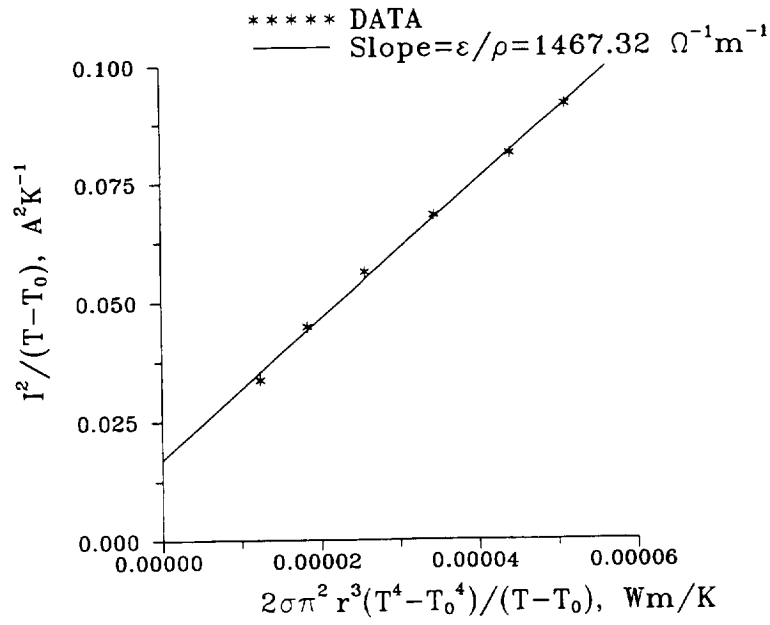

Figure 16
Plot of $I^2/(T-T_0)$ vs $2\sigma\pi^2r^3(T^4-T_0^4)/(T-T_0)$.

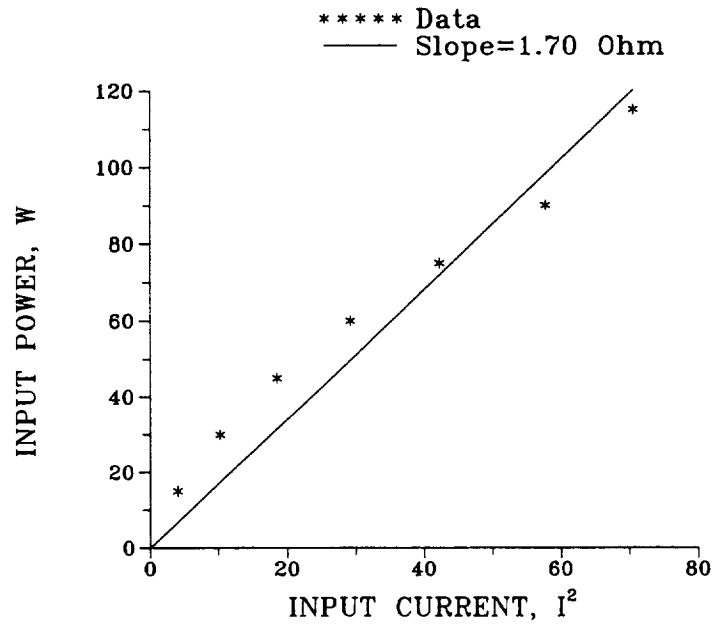

Figure 17
Plot of SiC heater input power vs square of input current.

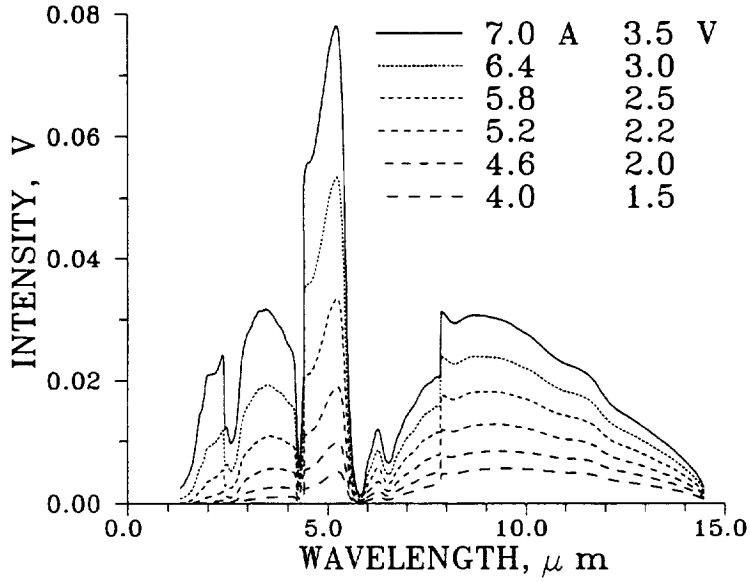

Figure 18
Voltage spectra of ceramic heater.

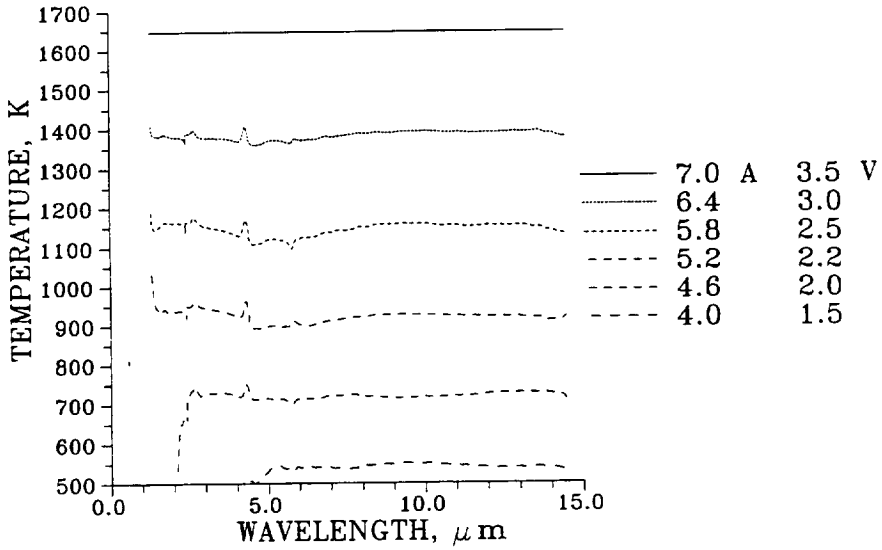

Figure 19
Average temperatures for different input currents and voltages.

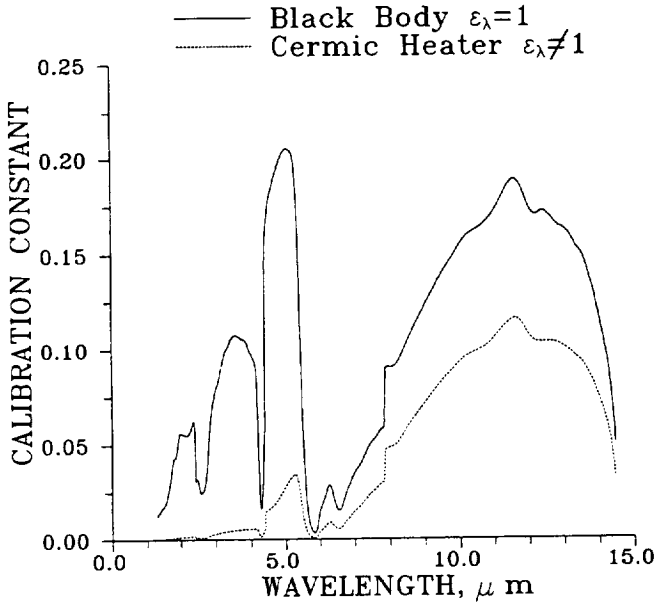

Figure 20
Calibration constants of the multiwavelength pyrometer for ceramic heater and black body furnace.

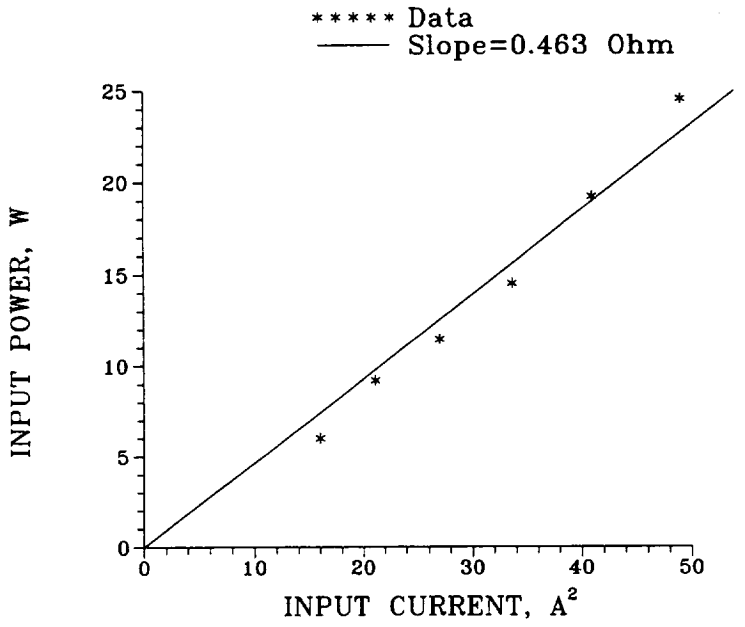

Figure 21
Plot of ceramic heater input power vs square of input current.

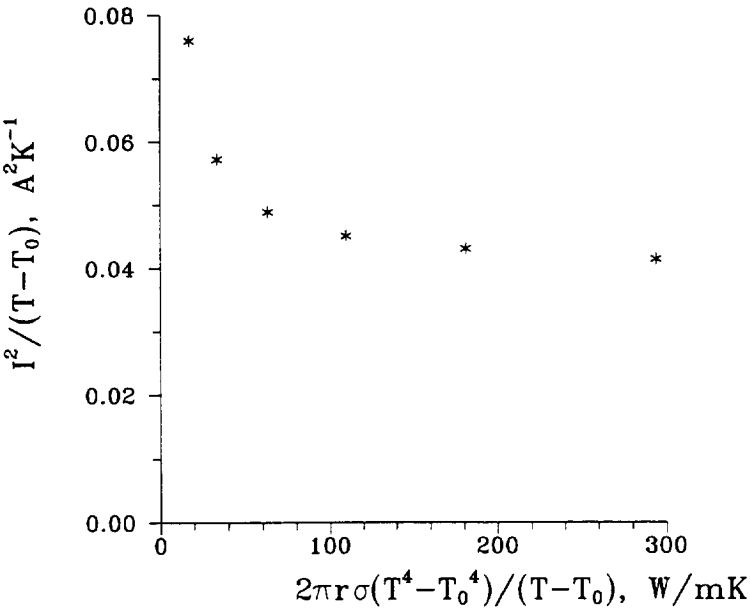

Figure 22
Plot of $I^2/(T-T_0)$ vs $2\pi r\sigma(T^4-T_0^4)/(T-T_0)$.

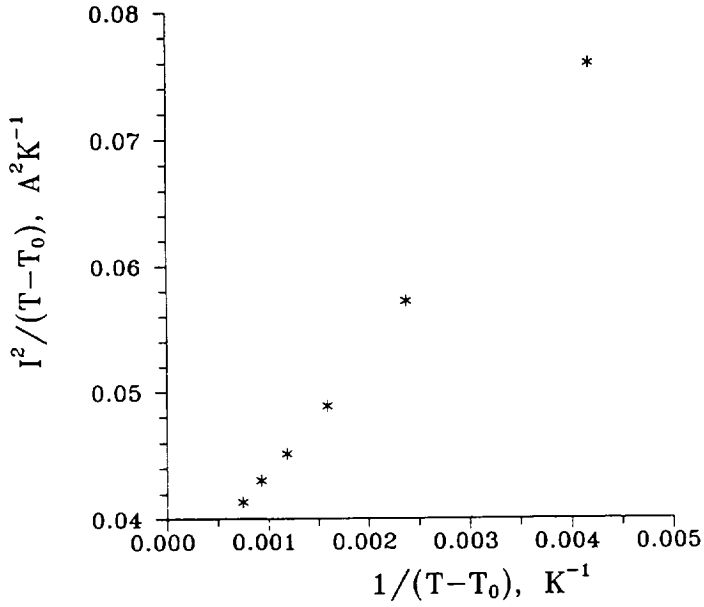

Figure 23
Plot of $I^2/(T-T_0)$ vs $1/(T-T_0)$.

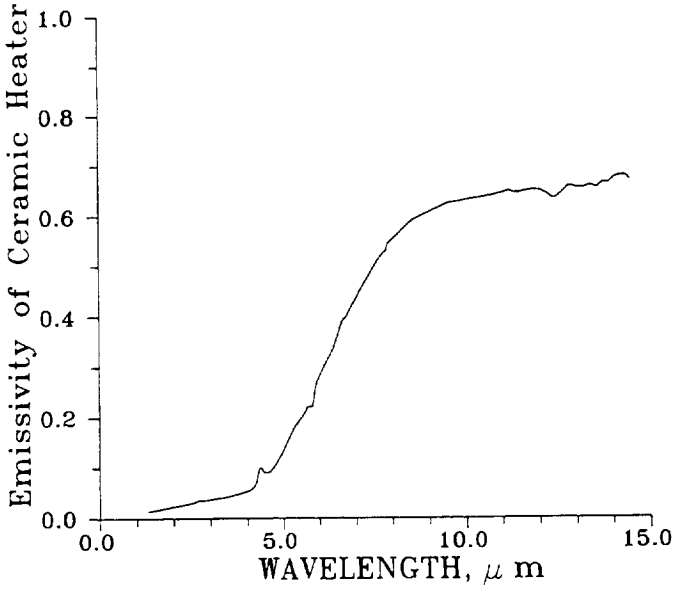

Figure 24
Emissivity of ceramic heater.

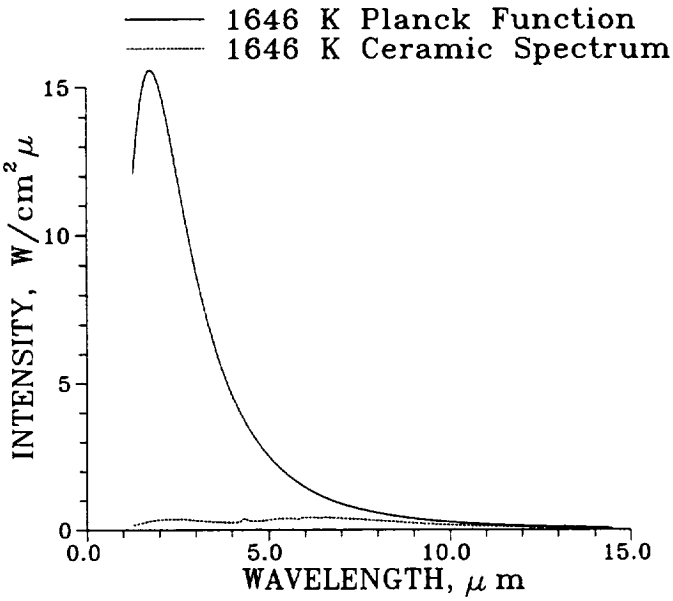

Figure 25
Free emitting black body curve and calculated ceramic heater emission curve.

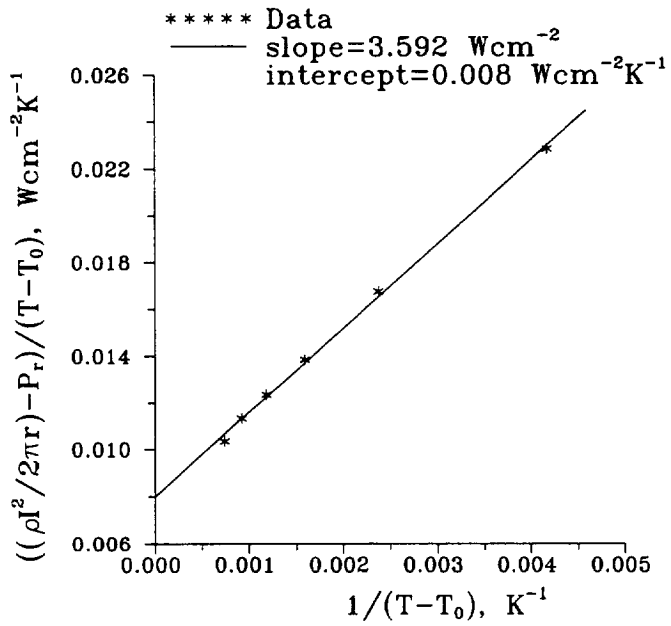

Figure 26
Plot of $(\rho I^2/2\pi r-P_r)/(T-T_0)$ vs $1/(T-T_0)$.

REPORT DOCUMENTATION PAGE

Form Approved
OMB No. 0704-0188

1. AGENCY USE ONLY (*Leave blank*)	2. REPORT DATE	3. REPORT TYPE AND DATES COVERED
	January 1996	Technical Memorandum

4. TITLE AND SUBTITLE

Application of the Self Calibrating Emissivity and/or Transmissivity Independent Multiwavelength Pyrometer to Measure the Temperatures of Tungsten and Refractory Material Surfaces

5. FUNDING NUMBERS

WU-505-90-51

6. AUTHOR(S)

Daniel Ng and Charles M. Spuckler

7. PERFORMING ORGANIZATION NAME(S) AND ADDRESS(ES)

National Aeronautics and Space Administration
Lewis Research Center
Cleveland, Ohio 44135-3191

8. PERFORMING ORGANIZATION REPORT NUMBER

E-10090

9. SPONSORING/MONITORING AGENCY NAME(S) AND ADDRESS(ES)

National Aeronautics and Space Administration
Washington, D.C. 20546-0001

10. SPONSORING/MONITORING AGENCY REPORT NUMBER

NASA TM-107152

11. SUPPLEMENTARY NOTES

Responsible person, Daniel Ng, organization code 2510, (216) 433-3638.

12a. DISTRIBUTION/AVAILABILITY STATEMENT

Unclassified - Unlimited
Subject Category 35

This publication is available from the NASA Center for Aerospace Information, (301) 621-0390.

12b. DISTRIBUTION CODE

13. ABSTRACT (*Maximum 200 words*)

The self calibrating emissivity and/or transmissivity independent multiwavelength pyrometer is ideally suited to measure the temperature of a surface when the emissivity of the surface and the transmissivity of the medium separating the surface from the pyrometer are either or both not known. Such is the case of the tungsten filament in a quartz lamp. Using a one-color pyrometer would require knowing the quartz lamp envelope transmissivity and the filament's emissivity to measure temperature. This information can only be obtained if samples of the filament and envelope are available. Assuming that these quantities are wavelength independent over a wavelength region, a ratioing 2-color pyrometer can measure the temperature, but the ratio signal is susceptible to noise. The disappearing filament pyrometer measures only a brightness temperature. It still needs the emissivity and transmissivity to make corrections to the measured temperature. The NASA self calibrating multiwavelength pyrometer is a recent addition to the list of pyrometers used in research and development. Its principle of operation makes it ideally suited to measure the temperature of surfaces without needing to know the emissivity of the surface, the transmissivity of the intervening medium or the calibration constant of the detector before hand. It has successfully measured the surface temperatures of tungsten, silicon carbide and refractory oxides in three infrared light sources. The measured temperatures are used to analyze the heat transfer in each case.

14. SUBJECT TERMS	15. NUMBER OF PAGES
Pyrometer; Tungsten; Silicon carbide; Ceramic; Heat transfer	22
	16. PRICE CODE: A03

17. SECURITY CLASSIFICATION OF REPORT	18. SECURITY CLASSIFICATION OF THIS PAGE	19. SECURITY CLASSIFICATION OF ABSTRACT	20. LIMITATION OF ABSTRACT
Unclassified	Unclassified	Unclassified	

National Aeronautics and
Space Administration

Lewis Research Center
21000 Brookpark Rd.
Cleveland, OH 44135-3191